

The effect of microstructure and film composition on the mechanical properties of linear antenna CVD diamond thin films

Rani Mary Joy ^{a,b,*}, Paulius Pobedinskas ^{a,b}, Nina Baule ^c, Shengyuan Bai ^d, Daen Jannis ^{e,f}, Nicolas Gauquelin ^{e,f}, Marie-Amandine Pinault-Thaury ^g, François Jomard ^g, Kamatchi Jothiramalingam Sankaran ^{a,b,2}, Rozita Rouzbahani ^{a,b}, Fernando Lloret ^{a,b,3}, Derese Desta ^{a,b}, Jan D'Haen ^{a,b}, Johan Verbeeck ^{e,f}, Michael Frank Becker ^c, Ken Haenen ^{a,b}

^a *Institute for Materials Research (IMO), Hasselt University, Wetenschapspark 1, B-3590 Diepenbeek, Belgium*

^b *IMOMECA, IMEC vzw, Wetenschapspark 1, B-3590 Diepenbeek, Belgium*

^c *Fraunhofer USA, Inc., Center Midwest, 1449 Engineering Research Ct, East Lansing, MI, 48824, USA*

^d *Dept. Chemical Engineering and Materials Science, Michigan State University, East Lansing, MI, 48823, USA*

^e *Electron Microscopy for Material Science (EMAT), University of Antwerp, Groenenborgerlaan 171, 2020 Antwerp, Belgium*

^f *NANOLab Centre of Excellence, University of Antwerp, Groenenborgerlaan 171, 2020 Antwerp, Belgium*

^g *Groupe d'Etude de la Matière Condensée (GEMaC-UMR8635), CNRS, Université de Versailles St-Quentin-En-Yvelines (UVSQ), Université Paris-Saclay, 45 av des Etats Unis, 78035 Versailles Cedex, France*

* Corresponding author at: Institute for Materials Research (IMO), Hasselt University, Wetenschapspark 1, B-3590 Diepenbeek, Belgium.

E-mail addresses: rani.maryjoy@uhasselt.be (R. Mary Joy), paulius.pobedinskas@uhasselt.be (P. Pobedinskas), ken.haenen@uhasselt.be (K. Haenen).

1 R. Mary Joy and Paulius Pobedinskas contributed equally to this work.

2 Currently at CSIR-Institute of Minerals and Materials Technology, Bhubaneswar 751013, India.

3 Currently at Dept. Applied Physics, Universidad de Cádiz, 11510 Puerto Real (Cádiz), Spain.

Abstract

This study reports the impact of film microstructure and composition on the Young's modulus and residual stress in nanocrystalline diamond (NCD) thin films (≈ 250 nm thick) grown on silicon substrates using a linear antenna microwave plasma-enhanced chemical vapor deposition (CVD) system. Combining laser acoustic wave spectroscopy to determine the elastic properties with simple wafer curvature measurements, a straightforward method to determine the intrinsic stress in NCD films is presented. Two deposition parameters are varied: (1) the substrate temperature from 400 °C to 900 °C, and (2) the [P]/[C] ratio from 0 ppm to 8090 ppm in the H₂ /CH₄ /CO₂ /PH₃ diamond CVD plasma. The introduction of PH₃ induces a transition in the morphology of the diamond film, shifting from NCD with larger grains to ultra-NCD with a smaller grain size, concurrently resulting in a decrease in Young's modulus. Results show that the highest Young's modulus of (1130 ± 50) GPa for the undoped NCD deposited at 800 °C is comparable to single crystal diamond, indicating that NCD with excellent mechanical properties is achievable with our process for thin diamond films. Based on the film stress results, we propose the origins of tensile intrinsic stress in the diamond films. In NCD, the tensile intrinsic stress is attributed to larger grain size, while in ultra-NCD films the tensile intrinsic stress is due to grain boundaries and impurities.

Keywords:

Linear antenna CVD reactor, Nanocrystalline diamond, Young's modulus, Residual stress, Phosphorus doping

1. Introduction

Owing to its superior mechanical and tribological properties, single crystal diamond is an attractive candidate used in various applications, however, high fabrication costs and limited up-scaling hinder its wide industrial usage [1,2]. Polycrystalline diamond, particularly nanocrystalline diamond (NCD) and ultra-NCD (UNCD), with the prospect of large area deposition on non-diamond substrates, is an alternative to single crystal diamond for many applications such as electrochemistry, sensing and microelectromechanical systems [3–5]. It is also very attractive for protective coatings, while high thermal conductivity makes NCD a strong candidate as heat spreaders on GaN devices thereby mitigating their reliability issues [6,7]. Despite these features, NCD is still limited in commercial usage due to its high process temperature leading to substrate damage and film adhesion issues. Of equal importance is the limited scalability in the conventional resonant cavity chemical vapor deposition (CVD) systems. Hot-filament CVD technique can be used for large area NCD, but it is restricted due to filament impurity incorporation and high growth temperature. By addressing these limitations, the surface wave microwave plasma-enhanced CVD (MW PE CVD) systems, operated with linear, distributed or slotted antennas, are promising alternatives and are capable to produce diamond coatings over large area and at lower temperature [8–10].

Concerning the diamond coatings, an essential property for thin film-based applications is the tunability of residual stress generated in the coatings. The main origins of residual stress in films are the thermal stress and intrinsic stress. Thus, the choice of substrate and deposition conditions determine the residual stress in thin films [11,12]. A wide range of values for the mechanical properties of diamond films and models for residual stress generation have been proposed [13–16]. Although large area NCD and UNCD can be achieved in the linear antenna (LA) MW PE CVD systems, very few studies focus on the mechanical properties of the films grown in such deposition systems [17,18]. Moreover, the determination of the Young's modulus of thin films is challenging as it involves the conversion of continuous NCD films into cantilevers or membranes for bulge tests and/or uses destructive techniques such as nanoindentation that are influenced by the film surface roughness and the underlying substrate [13,19]. In this study, we use an alternative non-destructive laser-induced surface acoustic wave technique for the Young's modulus analysis of diamond films. This technique does not require any sample preparation such as smoothing or cross-sectioning and is mostly conducted on the substrate/thin film systems used for the actual application. Compared to nanoindentation and as long as the materials allow the propagation of a sound wave, it can be applied to many thin film and surface layers, ranging from ultra-thin (<5 nm) to thick (several μm) from very hard to porous materials [20,21].

It is well known that doping enhances the electronic properties of diamond, the most common dopants

being boron and phosphorus, which make diamond a p- and n-type semiconductor, respectively. Most of previous studies report the diamond doping process using resonant cavity systems, while studies carried out by Taylor et al. report on boron-doped NCD layers in the LA MW PE CVD system [18,22,23]. Considering that diamond deposition in Ar or N₂ based plasma generates UNCD, it is also worth exploring how phosphine (PH₃) addition in the H₂/CH₄/CO₂ plasma influences film properties. However, no studies on phosphorus incorporation into NCD nor PH₃ addition as an impurity in the linear antenna system have been reported. Janssen et al. have demonstrated phosphorus incorporation in NCD under high substrate temperature conditions in resonant cavity system [24]. Hence, it is of interest to extend the study to high-temperature process conditions and investigate the possibility of n-type doping in LA MW PE CVD diamond films.

In this work, we report the first results on Young's modulus, film stress and phosphorus incorporation in LA MW PE CVD diamond films. We systematically investigate the morphological changes, film composition and correlate these properties with the residual stress in the (U)NCD thin films grown at various substrate temperatures and PH₃ concentrations in the CVD growth plasma. A control group of undoped diamond process at different substrate temperatures is also included, allowing us to decouple the influence of substrate temperature from PH₃ addition to the CVD plasma. By using a combination of two characterization techniques, laser surface acoustic wave and wafer curvature method, the Young's modulus and residual stress are measured in a simple and straightforward manner, allowing us to determine the origins of intrinsic stress, i.e. the process parameters to control the film stress are easily identified.

2. Experimental

Polished single crystal (100)-oriented 200 μm silicon substrates with an average roughness <0.5 nm were used for the experiments. Substrates with 1×1 cm² dimensions were used for all characterization techniques except for the laser-induced surface acoustic wave technique for which 2-inch silicon wafers were necessary. The substrates were dry-cleaned using an oxygen (O₂) gas discharge plasma [25].

After the treatment the substrates were seeded with nanodiamond (ND) particles by drop-casting a water-based ND colloid onto the substrate surface and covering it completely, followed by deionized water rinsing and spin-drying steps. The ND colloid was prepared from detonation ND slurry provided by the NanoCarbon Institute Co., Ltd, Japan. The size of the NDs is 5 to 7 nm and the zeta-potential of the colloid is (49 ± 5) mV.

The diamond films were deposited either using a gas mixture of H₂/CH₄/CO₂ (undoped), or with PH₃ addition to the gas mixture. The addition of CO₂ to the gas mixture was used to enhance the etching of

sp² carbon phase. The PH₃ gas precursor with a concentration of 1000 ppm in H₂ was used for the experiments. Three series of diamond growth experiments on the ND seeded substrates were done in the LA MW PE CVD reactor (Table 1). For each sample series, one deposition parameter was varied, i.e. [P]/[C] from 0 ppm (undoped) up to 8090 ppm at 400 °C for the PH₃-series, and substrate temperature (*T*) from 400 °C to 900 °C at [P]/[C] ratio of 8090 ppm (PH₃-T-series) or 0 ppm (undoped- T-series) gas compositions. The sample stage was heated by a resistive heater and *T* was measured by a thermocouple inside the stage. Before plasma ignition, the substrates were maintained at the set temperature. For all depositions the following parameters were kept constant: 5600 W of MW power in continuous wave mode, a working pressure of 22 Pa, a total gas flow of 150 sccm, a gas composition of 5% CH₄ and 6% CO₂ in H₂, and sample-to-antenna distance of 5 cm. The film thickness was monitored by in-situ laser reflection interferometry with a laser wavelength of 405 nm. Depending on the chosen process conditions, the film growth rate varied between 50 nm/h and 130 nm/h, hence the deposition time was adapted so that a total (U)NCD thin film thickness of about 250 nm was obtained for each sample.

Table 1 Overview of process variables in this study.

Experiment series	<i>T</i> (°C)	[P]/[C] (ppm)
PH ₃ -series	400	0 to 8090
PH ₃ -T-series	400 to 900	8090
Undoped-T-series	400 to 900	0

The samples chosen for transmission electron microscopy (TEM) were prepared using a FEI Helios 650 dual-beam Focused Ion Beam (FIB) device as a FIB lamella. Four-dimensional scanning TEM (4D STEM) was performed on a X-Ant-EM instrument operated at 300 keV. The 4D STEM experiment was performed by raster scanning an electron probe, with a convergence angle 1 mrad, and acquiring a diffraction pattern at every probe position with a resolution of about 2 nm.

The samples were characterized by confocal micro-Raman measurements using an argon ion laser ($\lambda_{exc.} = 488$ nm) with a Horiba Jobin Yvon T64000 spectrometer. Secondary ion mass spectrometry (SIMS) measurements (raster area of 150×150 μm²) were carried out on the sample deposited at a [P]/[C] ratio of 8090 ppm and substrate temperature of 900 °C to detect the impurities present in the film. Positive primary ions with a Cs⁺ source is set to 10 keV and an incidence angle of 23° with respect to the surface normal of the sample. The secondary ions are detected in the negative mode (sample bias at -5 kV).

X-ray reflectivity (XRR) was carried out for film density analysis with an X-ray diffraction (XRD, Rigaku SmartLab) system with monochromatized Cu K α 1 incident X-ray beam (1.541 Å). The measurement ranged from 0° to 2° with a step size of 0.0004° at 0.48°/min, whereas the analysis of the

diffraction patterns were performed between 0.4° to 0.6° with the GlobalFit software (Rigaku Ver.2.1.1). The material model for the fitting by the least mean square method consisted of a silicon substrate with an infinite thickness, a density of 2.33 g/cm^3 , roughness of 0.3 nm and an (U)NCD film thickness of 250 nm. The NCD density and roughness were subject to refinement, constraining the density between 2.00 g/cm^3 and 3.52 g/cm^3 . The apparent Young's modulus of the NCD films was determined by the laser surface acoustic wave technique (LAwave[®], Fraunhofer USA Center Midwest CMW) [26,27]. In this method, laser pulses ($\lambda = 337 \text{ nm}$, maximum power of 12 mW, pulse duration of 3 ns) absorbed by the substrate generate surface acoustic waves. The low power density of the laser pulse is sufficiently low for any change of state in the diamond film [28]. The waves propagate along the surface with amplitude decaying exponentially within the material. Due to this behavior, the surface acoustic wave is very sensitive to surface layers and modifications with elastic properties and density deviating from the bulk material. The penetration depth of the surface acoustic wave depends on frequency. The higher the frequency the lower the penetration depth. This method can be applied for thin films that are thinner than 50 nm. The wave signal was recorded with a 500 MHz digital oscilloscope averaged over 64 pulses in a frequency range from 40 MHz to 200 MHz and a scan length of 20 mm. The dispersion of the surface acoustic waves is a function of the substrate and film thickness, Poisson's ratio, film density and the Young's modulus. The applied material model consists of the substrate and film properties. The substrate properties were determined from an uncoated reference wafer. Due to linear dispersion for the investigated diamond films, fitting of only one unknown – the Young's modulus of the diamond film could be achieved. Hence, for all LAwave[®] measurements in this study, the Poisson's ratio of the films was set to 0.12 (Fig. S1) [29]. The film density values for each sample were derived from XRR measurements. Using the method of non-linear least squares curve fitting the Young's modulus of the diamond thin films was determined.

The in-plane residual stress component in the films was calculated by the Stoney equation [30–32]. The substrate curvatures before and after diamond CVD were obtained from line scans measurements with a Bruker DekTakXT[®] stylus profilometer. The elastic constants of the Si substrate were taken from the literature [33].

3. Results

3.1. Film morphology and composition

Fig. 1 shows the 4D-STEM correlation coefficient maps and the corresponding cross-sectional SEM images of four samples in this study. The samples are diamond thin films deposited at substrate temperature of

400 °C or 900 °C and with the lowest [P]/[C] ratio of 0 ppm (undoped) or the highest [P]/[C] ratio of 8090 ppm. The correlation coefficient maps are constructed from the differences between neighboring diffraction patterns, with the white regions in the STEM images indicating grain boundaries. Of the four samples, the undoped 400 °C sample (Fig. 1(a)) has the largest grains with least grain boundaries. In contrast, the [P]/[C] = 8090 ppm sample deposited at 400 °C (Fig. 1(b)) shows a complex microstructure with significantly smaller grains and more grain boundaries. Thus, it can be confirmed that addition of PH₃ at a [P]/[C] ratio of 8090 ppm to the diamond CVD plasma leads to grain size reduction. A gradual film morphology transition, from faceted to dendrite-like features with smaller grains, with increasing [P]/[C] ratio (PH₃-series at 400 °C) can be seen in Figure S2(a). A reduced grain size is also observed for the undoped sample deposited at 900 °C (Fig. 1(c)). In this case, the grain size reduction is observed only at the highest substrate temperature of 900 °C (Figs S2(c) and S3). The NCD film grown with the highest [P]/[C] ratio at 900 °C (Fig. 1(d)) also has a complex morphology. While clusters of smaller diamond grains are observed, there are no notable distinctions compared to the film deposited at 400 °C with the highest [P]/[C] ratio.

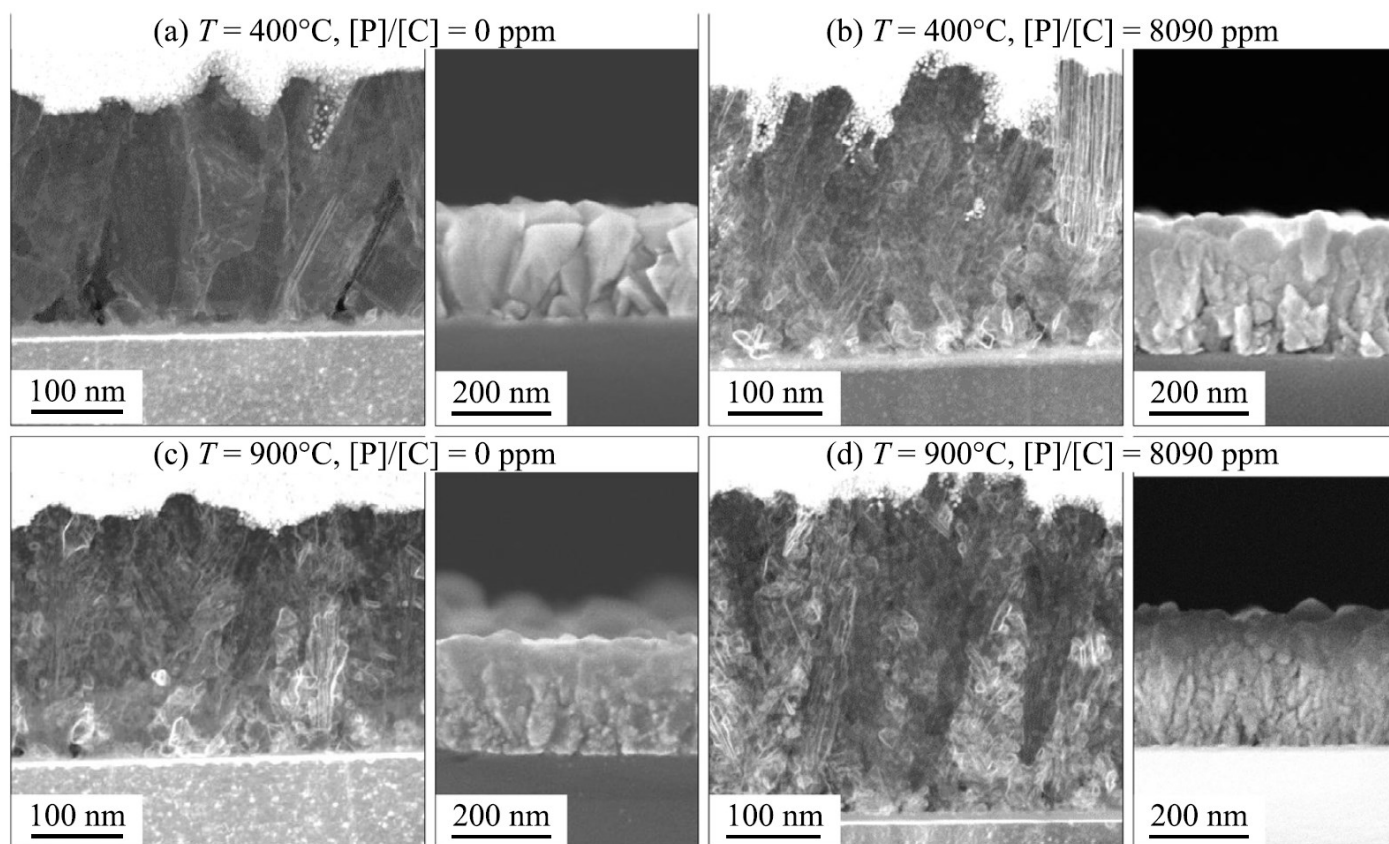


Fig. 1. (a-d) 4D-STEM correlation coefficient maps (left) and cross-sectional SEM (right) images of the diamond films deposited with [P]/[C] ratio of 0 ppm and 8090 ppm at 400 °C and 900 °C, respectively. The white lines indicate the presence of grain boundaries.

In addition to the morphology change, the diamond content of the films also changes with the growth conditions. Fig. 2 shows the diamond content in the films qualitatively estimated from the Raman spectra of the samples (Fig. S4). The sp^3 content remains almost constant at $(80 \pm 10)\%$ for the PH_3 -series samples (Fig. 2(a)). As expected from the faceted morphology, the undoped diamond films showed the highest amount of sp^3 bonded carbon ($\approx 90\%$) with the maximum from $500\text{ }^\circ\text{C}$ to $700\text{ }^\circ\text{C}$ (Fig. 2(b)). Both the temperature series samples show similar trends — an increase in temperature above $800\text{ }^\circ\text{C}$ leads to a significant reduction in the amount of sp^3 bonded carbon ($\approx 40\%$) for both $[P]/[C] = 8090$ ppm and the undoped layers and increasing growth rate of the diamond films (Fig. 2(c)).

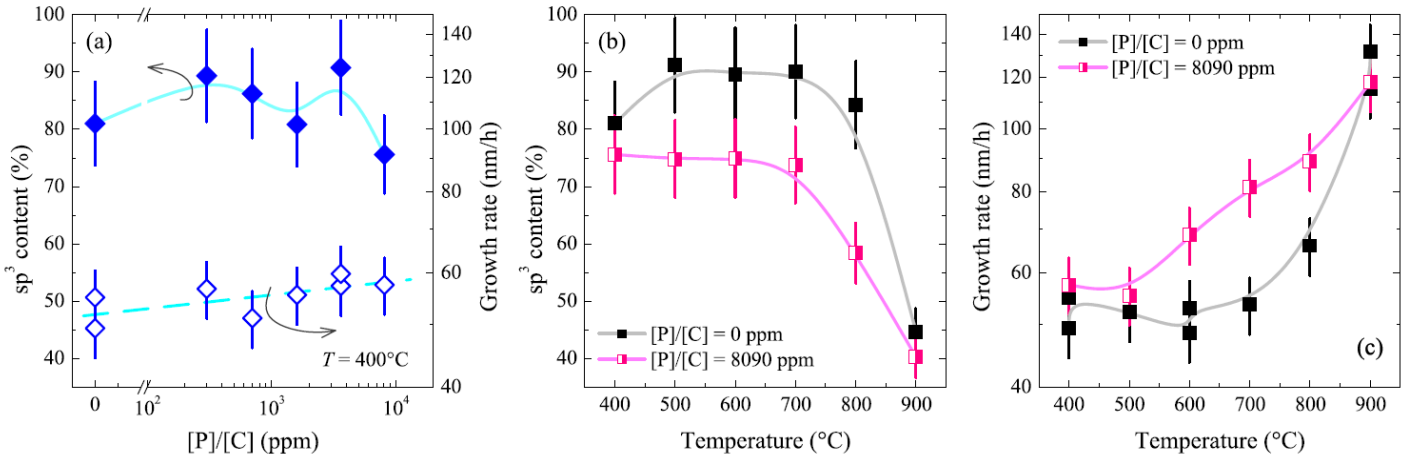


Fig. 2. (a) sp^3 content in PH_3 -series samples grown at $T = 400\text{ }^\circ\text{C}$ and their respective growth rates. The sp^3 content (b) in PH_3 -T-series and undoped-T-series samples, and their corresponding growth rates (c).

Thus far, phosphorus is reported to successfully incorporate in diamond layers only at elevated temperature ($>800\text{ }^\circ\text{C}$) [24,34]. Hence, the sample deposited at $[P]/[C] = 8090$ ppm and at a substrate temperature of $900\text{ }^\circ\text{C}$ was chosen for SIMS analysis (Fig. 3). The depth profiling results show phosphorus incorporation with uniform concentration throughout the thickness of the diamond layer. Although this result confirms that phosphorus is present in the bulk and in high concentration ($4.2 \times 10^{19}\text{ cm}^{-3}$), it should be kept in mind that impurities are known to incorporate in grain boundaries and in non-diamond phases [35–37]. Hence, it may not be representative of the actual phosphorus concentration within the diamond grain. Additional impurities detected in the film are H, O, Si, N and B. All impurities except boron are present in high levels ($>5 \times 10^{18}\text{ cm}^{-3}$). The presence of silicon and oxygen is attributed to the quartz tube etching during the CVD process [8], while residual N present in the deposition chamber is due to the base pressure (1×10^{-4} mbar) of the deposition system. The boron concentration, between $6 \times 10^{16}\text{ cm}^{-3}$ and $6 \times 10^{17}\text{ cm}^{-3}$, is unexpected as there is no boron dopant

source in the process. Hence, its origin is unclear. In addition to SIMS, measurements carried out with EDX and XPS techniques also confirm the variations in film composition among samples grown with different deposition conditions (Figs S5 and S6). Thus, from the above results it can be inferred that the film microstructure as well as the film composition change with the CVD diamond growth conditions.

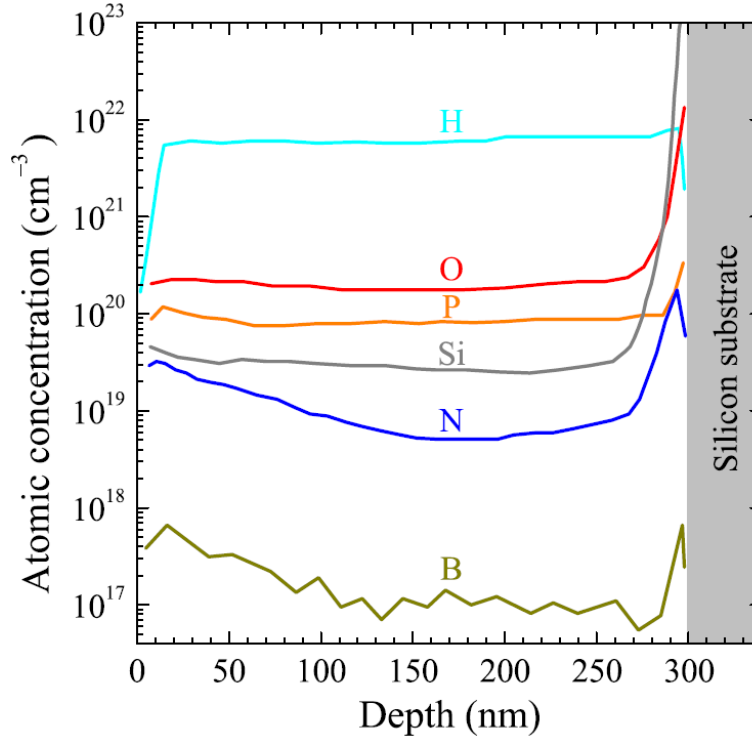


Fig. 3. SIMS depth profile of the diamond film deposited with [P]/[C] ratio of 8090 ppm at 900 °C.

3.2. Young's modulus and in-plane residual stress

The Young's modulus (E) of the diamond films also varies with the deposition conditions (Fig. 4). The values of E are between (450 ± 50) GPa and (1130 ± 50) GPa, with the highest for the undoped NCD layers. The PH_3 -series samples have almost constant E values of ≈ 630 GPa except for the highest [P]/[C] ratio where a drop to ≈ 450 GPa is observed (Fig. 4(a)). For the undoped-T-series films, E steadily increases until 800 °C and sharply reduces at the highest substrate temperature of 900 °C (Fig. 4(b)). On the other hand, the increasing substrate temperature has a negligible effect on E for the PH_3 -T-series up to 700 °C beyond which an increase is observed. It should be noted that the highest values of E for the undoped diamond sample is comparable to that of single crystal diamond and achieved in our process with thin NCD films. Fig. 4(d) shows the Young's modulus as a function of the diamond film density as determined with the XRR technique. The average film density of (3.46 ± 0.06) g/cm³ for the undoped-T-series samples is comparable to that of single crystal diamond (3.52 g/cm³). The PH_3 -series films have a

density of $(3.27 \pm 0.07) \text{ g/cm}^3$ while no clear trend is observed for the PH_3 -T-series samples.

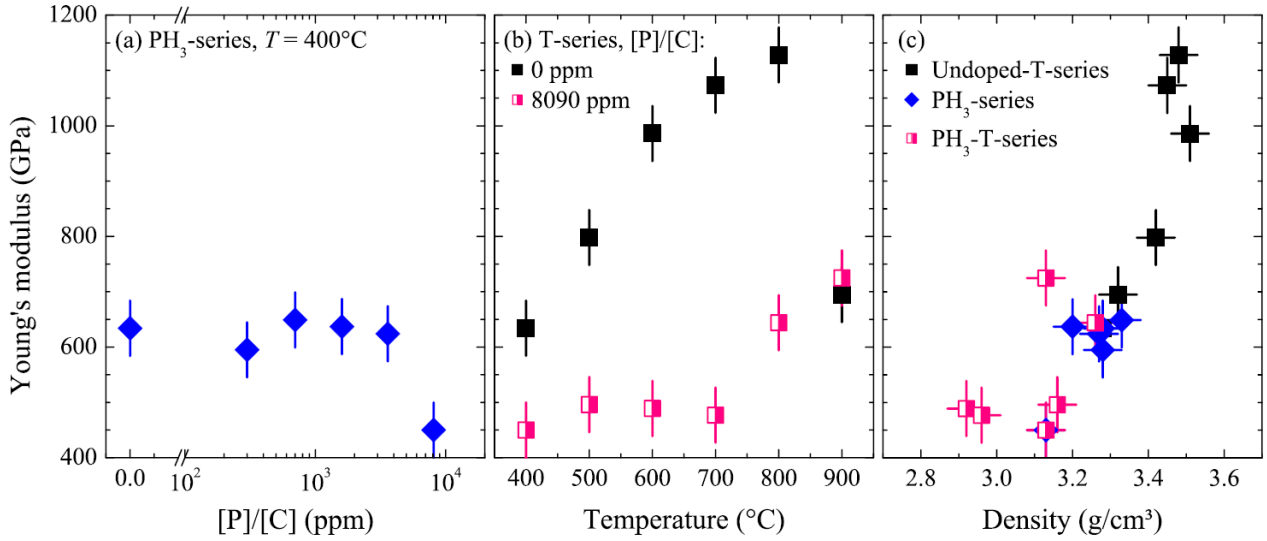


Fig. 4. Young's modulus of the diamond thin films: (a) PH_3 -series, (b) PH_3 -T-series and undoped-T-series, and (c) Young's modulus as a function of film density.

Fig. 5 shows the in-plane residual, thermal and intrinsic stress for the deposited films. The in-plane residual stress in the diamond films is evaluated from the wafer curvature measurements. All samples have compressive residual stress with the lowest value of -0.25 GPa for the film grown at $[\text{P}]/[\text{C}]$ ratio of 8090 ppm and at a substrate temperature of $900 \text{ }^\circ\text{C}$. In general, the origins of the residual stress in thin films are due to: (i) the mismatch between the lattices of the substrate and the film, (ii) the thermal expansion coefficient difference, which generates the thermal stress when cooling down to room temperature after deposition, and (iii) the intrinsic stress, which depends on the CVD deposition conditions [11]. As the diamond growth occurs on ND seeds and not directly on the silicon substrate, the lattice mismatch is not considered in this study. The thermal stress (σ) is expressed as:

$$\sigma = \frac{E}{1 - \nu} (\alpha_{\text{film}} - \alpha_{\text{sub.}}) (T - T_0) \quad (1)$$

with E and ν the Young's modulus and the Poisson's ratio of NCD, respectively, α_{film} and $\alpha_{\text{sub.}}$ the thermal expansion coefficients of thin film and substrate, respectively, T and T_0 the substrate temperature at film deposition and room temperature, respectively. The thermal expansion coefficient values are reported in literature [38], and Young's modulus values were experimentally determined. The Young's modulus values stayed almost constant with Poisson's ratio (Fig. S1), hence a Poisson's ratio of 0.12 was chosen for Young's modulus determination as well as for thermal stress calculations [29,39].

Once the thermal stress for each deposition is calculated, it can be subtracted from the residual stress giving the value of the intrinsic stress, which can then be correlated with the film properties.

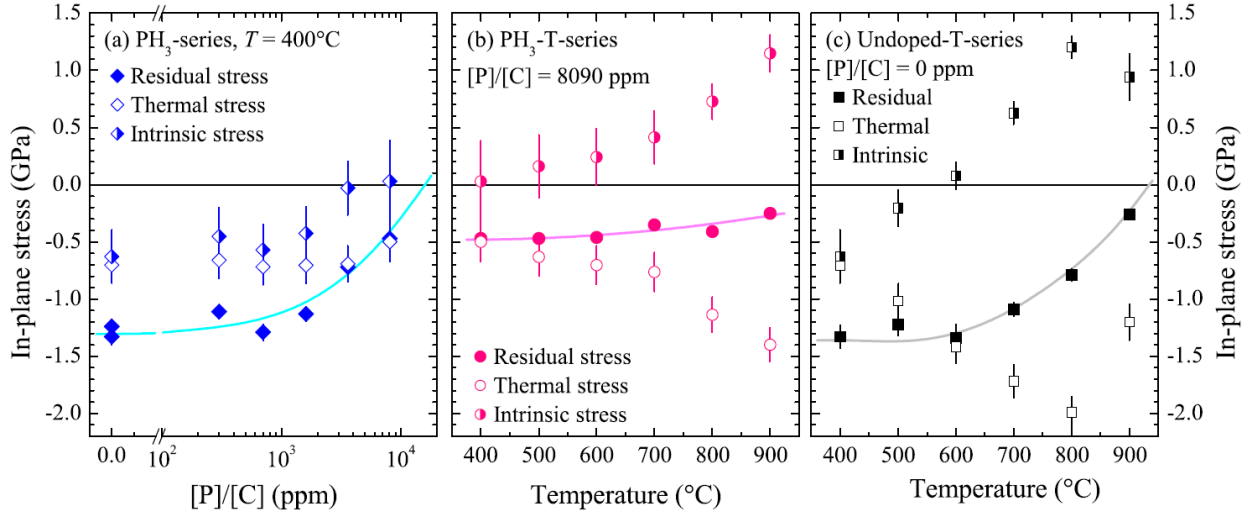


Fig. 5. In-plane residual, thermal and intrinsic stress of the (U)NCD films: (a) PH₃-series, (b) PH₃-T-series, and (c) undoped-T-series.

For the PH₃-series, the deposition temperature is constant (400 °C) and E values remain almost constant (≈ 630 GPa), except for the sample deposited at the highest [P]/[C] ratio. Therefore, the calculated thermal stress is compressive and vary between -0.34 GPa and -0.36 GPa for all PH₃-series samples except at the highest [P]/[C] ratio for which it is -0.25 GPa. With the increase in substrate temperature, the thermal stress increases systematically for both of the T-series, except for the undoped film at 900 °C. Again, this deviation is due to the drop in the value of Young's modulus. The evaluated intrinsic stress is compressive for the PH₃-series and decreases with increasing [P]/[C] ratio. While, a transition from compressive to tensile intrinsic stress is observed at 400 °C and 600 °C for the PH₃-T-series and undoped-T-series, respectively.

4. Discussion

4.1. Film morphology and film composition

Depending on the CVD process conditions, the samples have different microstructure, ranging from randomly faceted NCD to a cauliflower-like film with finer grains of ultra-NCD. The UNCD process reported earlier in N₂-based, Ar-based, or CH₄-rich plasmas is primarily attributed to impurity-related surface processes due to changes in plasma chemistry and surface kinetics resulting in smaller grains [40–42]. In our samples, the morphology transition for the PH₃-series samples confirms that phosphine-based CVD diamond growth plasma with [P]/[C] ratio of 8090 ppm in the linear antenna CVD system is an

impurity driven process. As comparable morphology changes is observed for the undoped layers at 900 °C, we propose that additional impurities, such as residual gases in the chamber, may be introduced into the H₂/CH₄/CO₂ diamond growth plasma at higher stage temperature. Therefore, the complex morphology featuring clusters of smaller diamond grains (Fig. 1(d)) is suggested to originate from the introduction of phosphine and other impurities into the CVD growth plasma at 900 °C. Moreover, impurities such as silicon are also known to originate from the quartz tubes of the CVD system [8], leading to plate-like morphology (Fig. S2). Whether these impurities play a role in UNCD formation at higher deposition temperature (900 °C), leading to transition in the film morphology, remains under investigation.

Earlier studies in the literature report increased sp³ content in diamond films fabricated at higher substrate temperature in the resonant cavity MW PE CVD reactor [43,44] and LA MW PE CVD reactor [45]. Our results are contrary — the samples have lower sp³ bonded carbon content at the highest substrate temperature and can be explained by the impurity driven transition to UNCD process [46,47].

4.2. Young's modulus and in-plane residual stress

The Young's modulus values obtained for the diamond films can be elucidated by considering the projected grain areas (deduced from the SEM images, Fig. S2). All values, except for the increased E at 800 °C and 900 °C for the PH₃-T-series, correlate well with the corresponding projected diamond grain areas, with higher E for larger grain areas (Fig. 6(a)). Thus, it can be confirmed that the Young's modulus of the diamond films depends on the CVD process conditions. Prior reports on NCD process, associate lower Young's modulus with smaller grains (i.e. more grain boundaries) [13,14,19,48]. A theoretical study by Sha et al. shows a direct correlation between the decrease in Young's modulus and the increase in the density of grain boundaries in UNCD [49], while Fallon et al. using TEM, observed amorphous carbon at the grain boundaries and at the edges of the CVD diamond grains [50]. We can hence expect that diamond films with smaller grains, thus with a higher fraction of grain boundaries and amorphous carbon, result in a lower Young's modulus than samples with larger grains and less grain boundaries.

The intrinsic stress of diamond films is dependent on the CVD conditions — the film morphology, impurities and grain boundaries are known to impact the intrinsic stress of the grown film [51]. It is generally accepted that the compressive intrinsic stress is attributed to non-diamond phases, hydrogen content and/or impurities in the layer [52]. Tensile intrinsic stress in diamond films are reported to be generated by dislocations, voids and grain boundaries explained using the grain boundary model [16,52,53]. The PH₃-series samples exhibit compressive intrinsic stress, with a non-diamond content of less than 20%. However, the samples with even higher non-diamond content, such as those deposited

at 900 °C, display tensile intrinsic stress. These observations are contrary to the expected results; hence the non-diamond content alone cannot explain the origins of intrinsic stress.

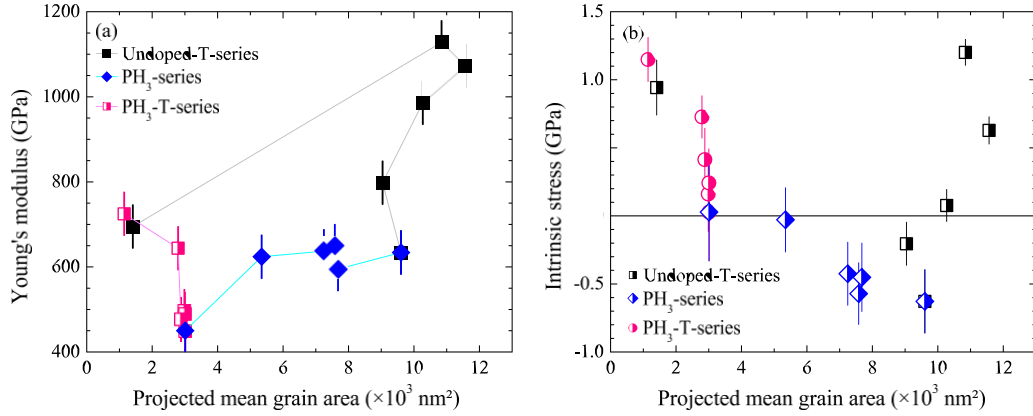


Fig. 6. (a) Young's modulus and (b) intrinsic stress as a function of the projected grain area for the diamond thin films.

In our samples, we explain the origins of intrinsic stress on the basis of film microstructure. Our results (Fig. 6(b)) show undoped- T-series samples with largest grain areas have tensile intrinsic stress. High quality diamond with tensile stress are reported to arise from the onset of grain growth [12]. On the contrary, it can be seen that as the area of grains reduces (density of grain boundaries rises), the tensile intrinsic stress dominates, and the samples with the smallest grain area demonstrate the highest tensile stress. Thus, the presence of grain boundaries generating tensile stress can be supported. The incorporation of trans-polyacetylene (TPA) in UNCD films with smaller grains also generates tensile intrinsic stress [54]. The PH₃-T-series samples have prominent TPA peak in the Raman spectra (Fig. S4) and also contribute to the intrinsic tensile stress formation. The film density variation between $(2.92 \pm 0.05) \text{ g/cm}^3$ and $(3.13 \pm 0.05) \text{ g/cm}^3$ for the PH₃-T-series samples indicate film composition differences, i.e. changes in the carbon matrix surrounding the grains occur. We can hence conclude that tensile intrinsic stress is generated in high quality films with larger grains, while in UNCD the presence of grain boundaries, the incorporation of TPA and impurities in matrix surrounding the grains contribute to tensile intrinsic stress generation in the samples.

5. Conclusion

In this study, we systematically investigated the Young's modulus and residual stress of diamond films deposited with the linear antenna CVD system. The main conclusions are summarized as follows:

1. The linear antenna CVD system can be used for the growth of NCD with enhanced mechanical

- properties. The 250 nm thick undoped NCD films grown at 800 °C had the Young's modulus of (1130 ± 50) GPa and density of (3.46 ± 0.05) g/cm³, which are comparable to single crystal diamond.
2. The addition of PH₃ to the H₂/CH₄/CO₂ diamond CVD plasma leads to diamond films with reduced grain size, which is the cause of the Young's modulus reduction due to amorphous carbon within the grain boundaries.
 3. Tensile intrinsic stress in diamond films is microstructure-dependent and generated with higher magnitudes either in films with the smallest grain areas or in those with the largest grains. Additionally, the incorporation of TPA contribute to the tensile stress generation.
 4. The incorporation of phosphorus in NCD thin films with a concentration of up to 4.2×10^{19} cm⁻³ as shown by SIMS analysis marks a significant milestone for linear antenna type CVD systems. These findings pave the way for advancing to the next stages in fabricating large area phosphorus-doped diamond films.

Declaration of competing interest

The authors declare that they have no known competing financial interests or personal relationships that could have appeared to influence the work reported in this paper.

Acknowledgments

This work was financially supported by the Special Research Fund (BOF) via Methusalem NANO network, the Research Foundation – Flanders (FWO) via Project G0D4920N, and the CORNET project nr 263-EN ‘‘ULTRAHARD: Ultrahard optical diamond coatings’’ (2020–2021).

Appendix A. Supplementary data

Supplementary material related to this article can be found online at <https://doi.org/10.1016/j.actamat.2023.119548>.

References

- [1] J.-C. Arnault, S. Saada, V. Ralchenko, Chemical vapor deposition single-crystal diamond: A review, *Phys. Status Solidi RRL* 16 (1) (2022) 2100354, <http://dx.doi.org/10.1002/pssr.202100354>.
- [2] M. Schreck, *Growth of Single Crystal Diamond Wafers for Future Device Applications*, Ch. 20, John Wiley & Sons, Ltd, 2021, pp. 583–631, <http://dx.doi.org/10.1002/9783527824724.ch20>.

- [3] N. Yang, J.S. Foord, X. Jiang, Diamond electrochemistry at the nanoscale: A review, *Carbon* 99 (2016) 90–110, <http://dx.doi.org/10.1016/j.carbon.2015.11.061>.
- [4] S. Drijkoningen, S.D. Janssens, P. Pobedinskas, S. Koizumi, M.K. Van Bael, K. Haenen, The pressure sensitivity of wrinkled B-doped nanocrystalline diamond membranes, *Sci. Rep.* 6 (1) (2016) <http://dx.doi.org/10.1038/srep35667>.
- [5] O. Auciello, D.M. Aslam, Review on advances in microcrystalline, nanocrystalline and ultrananocrystalline diamond films-based micro/nano-electromechanical systems technologies, *J. Mater. Sci.* 56 (12) (2021) 7171–7230, <http://dx.doi.org/10.1007/s10853-020-05699-9>.
- [6] L. Vandenbulcke, M. De Barros, Deposition, structure, mechanical properties and tribological behavior of polycrystalline to smooth fine-grained diamond coatings, *Surf. Coat. Technol.* 146–147 (2001) 417–424, [http://dx.doi.org/10.1016/S0257-8972\(01\)01407-4](http://dx.doi.org/10.1016/S0257-8972(01)01407-4).
- [7] Y. Zhou, R. Ramaneti, J. Anaya, S. Korneychuk, J. Derluyn, H. Sun, J. Pomeroy, J. Verbeeck, K. Haenen, M. Kuball, Thermal characterization of polycrystalline diamond thin film heat spreaders grown on GaN HEMTs, *Appl. Phys. Lett.* 111 (4) (2017) 041901, <http://dx.doi.org/10.1063/1.4995407>.
- [8] S. Drijkoningen, P. Pobedinskas, S. Korneychuk, A. Momot, Y. Balasubramaniam, M.K. Van Bael, S. Turner, J. Verbeeck, M. Nesládek, K. Haenen, On the origin of diamond plates deposited at low temperature, *Cryst. Growth Des.* 17 (8) (2017) 4306–4314, <http://dx.doi.org/10.1021/acs.cgd.7b00623>.
- [9] H.-A. Mehedi, J. Achard, D. Rats, O. Brinza, A. Tallaire, V. Mille, F. Silva, C. Provent, A. Gicquel, Low temperature and large area deposition of nanocrystalline diamond films with distributed antenna array microwave-plasma reactor, *Diam. Relat. Mater.* 47 (2014) 58–65, <http://dx.doi.org/10.1016/j.diamond.2014.05.004>.
- [10] J. Zalieckas, P. Pobedinskas, M.M. Greve, K. Eikehaug, K. Haenen, B. Holst, Large area microwave plasma CVD of diamond using composite right/left-handed materials, *Diam. Relat. Mater.* 116 (2021) 108394, <http://dx.doi.org/10.1016/j.diamond.2021.108394>.
- [11] C.T. Kuo, C.R. Lin, H.M. Lien, Origins of the residual stress in CVD diamond films, *Thin Solid Films* 290–291 (1996) 254–259, [http://dx.doi.org/10.1016/S0040-6090\(96\)09016-5](http://dx.doi.org/10.1016/S0040-6090(96)09016-5).
- [12] N. Shang, C. Lee, Z. Lin, I. Bello, S. Lee, Intrinsic stress evolution in diamond films prepared in a CH₄–H₂–NH₃ hot filament chemical vapor deposition system, *Diam. Relat. Mater.* 9 (7) (2000) 1388–1392, [http://dx.doi.org/10.1016/S0925-9635\(00\)00265-X](http://dx.doi.org/10.1016/S0925-9635(00)00265-X).
- [13] O. Williams, A. Kriele, J. Hees, M. Wolfer, W. Müller-Sebert, C. Nebel, High Young's modulus in ultra thin nanocrystalline diamond, *Chem. Phys. Lett.* 495

- (1) (2010) 84–89, <http://dx.doi.org/10.1016/j.cplett.2010.06.054>.
- [14] M. Mohr, A. Caron, P. Herbeck-Engel, R. Bennewitz, P. Gluche, K. Brühne, H.-J. Fecht, Young's modulus, fracture strength, and Poisson's ratio of nanocrystalline diamond films, *J. Appl. Phys.* 116 (12) (2014) 124308, <http://dx.doi.org/10.1063/1.4896729>.
- [15] C. Hua, X. Yan, J. Wei, J. Guo, J. Liu, L. Chen, L. Hei, C. Li, Intrinsic stress evolution during different growth stages of diamond film, *Diam. Relat. Mater.* 73 (2017) 62–66, <http://dx.doi.org/10.1016/j.diamond.2016.12.008>.
- [16] W.L. Wang, M.C. Polo, G. Sánchez, J. Cifre, J. Esteve, Internal stress and strain in heavily boron-doped diamond films grown by microwave plasma and hot filament chemical vapor deposition, *J. Appl. Phys.* 80 (3) (1996) 1846–1850, <http://dx.doi.org/10.1063/1.362996>.
- [17] S.S. Nicley, S. Drijkoningen, P. Pobedinskas, J. Raymakers, W. Maes, K. Haenen, Growth of boron-doped diamond films on gold-coated substrates with and without gold nanoparticle formation, *Cryst. Growth Des.* 19 (6) (2019) 3567–3575, <http://dx.doi.org/10.1021/acs.cgd.9b00488>.
- [18] A. Taylor, L. Klimša, J. Kopeček, Z. Remeš, M. Vronka, R. Čtvrtlík, J. Tomáščík, V. Mortet, Synthesis and properties of diamond - silicon carbide composite layers, *J. Alloys Compd.* 800 (2019) 327–333, <http://dx.doi.org/10.1016/j.jallcom.2019.06.016>.
- [19] M. Wiora, K. Brühne, A. Flöter, P. Gluche, T. Willey, S. Kucheyev, A. Van Buuren, A. Hamza, J. Biener, H.-J. Fecht, Grain size dependent mechanical properties of nanocrystalline diamond films grown by hot-filament CVD, *Diam. Relat. Mater.* 18 (5) (2009) 927–930, <http://dx.doi.org/10.1016/j.diamond.2008.11.026>.
- [20] D. Schneider, P. Siemroth, T. Schülke, J. Berthold, B. Schultrich, H.-H. Schneider, R. Ohr, B. Petereit, H. Hillgers, Quality control of ultra-thin and super-hard coatings by laser-acoustics, *Surf. Coat. Technol.* 153 (2) (2002) 252–260, [http://dx.doi.org/10.1016/S0257-8972\(01\)01664-4](http://dx.doi.org/10.1016/S0257-8972(01)01664-4).
- [21] G. Chow, E. Uchaker, G. Cao, J. Wang, Laser-induced surface acoustic waves: An alternative method to nanoindentation for the mechanical characterization of porous nanostructured thin film electrode media, *Mech. Mater.* 91 (2015) 333–342, <http://dx.doi.org/10.1016/j.mechmat.2015.10.005>.
- [22] A. Taylor, L. Fekete, P. Hubík, A. Jäger, P. Janíček, V. Mortet, J. Mistrík, J. Vacík, Large area deposition of boron doped nano-crystalline diamond films at low temperatures using microwave plasma enhanced chemical vapour deposition with linear antenna delivery, *Diam. Relat. Mater.* 47 (2014) 27–34, <http://dx.doi.org/10.1016/j.diamond.2014.05.002>.

- [23] A. Taylor, P. Ashcheulov, P. Hubík, L. Klimša, J. Kopeček, Z. Remeš, Z. Vlčková Živcová, M. Remzová, L. Kavan, E. Scheid, J. Lorinčík, V. Mortet, Precursor gas composition optimisation for large area boron doped nano-crystalline diamond growth by MW-la-PECVD, *Carbon* 128 (2018) 164–171, <http://dx.doi.org/10.1016/j.carbon.2017.11.063>.
- [24] W. Janssen, S. Turner, G. Sakr, F. Jomard, J. Barjon, G. Degutis, Y.-G. Lu, J. D’Haen, A. Hardy, M.V. Bael, J. Verbeeck, G.V. Tendeloo, K. Haenen, Substitutional phosphorus incorporation in nanocrystalline CVD diamond thin films, *Phys. Status Solidi RRL* 8 (8) (2014) 705–709, <http://dx.doi.org/10.1002/pssr.201409235>.
- [25] P. Pobedinskas, G. Degutis, W. Dexters, W. Janssen, S.D. Janssens, B. Conings, Ruttens, J. D’Haen, H.-G. Boyen, A. Hardy, M.K. Van Bael, K. Haenen, Surface plasma pretreatment for enhanced diamond nucleation on AlN, *Appl. Phys. Lett.* 102 (20) (2013) 201609, <http://dx.doi.org/10.1063/1.4807591>.
- [26] D. Schneider, B. Schultrich, H.-J. Scheibe, H. Ziegele, M. Griepentrog, A laser-acoustic method for testing and classifying hard surface layers, *Thin Solid Films* 332 (1–2) (1998) 157–163, [http://dx.doi.org/10.1016/s0040-6090\(98\)00988-2](http://dx.doi.org/10.1016/s0040-6090(98)00988-2).
- [27] D. Schneider, T. Schwarz, H.-J. Scheibe, M. Panzner, Non-destructive evaluation of diamond and diamond-like carbon films by laser induced surface acoustic waves, *Thin Solid Films* 295 (1–2) (1997) 107–116, [http://dx.doi.org/10.1016/s0040-6090\(96\)09163-8](http://dx.doi.org/10.1016/s0040-6090(96)09163-8).
- [28] J. Aussel, A. Le Brun, J. Baboux, Generating acoustic waves by laser: theoretical and experimental study of the emission source, *Ultrasonics* 26 (5) (1988) 245–255, [http://dx.doi.org/10.1016/0041-624x\(88\)90013-3](http://dx.doi.org/10.1016/0041-624x(88)90013-3).
- [29] Z.H. Shen, P. Hess, J.P. Huang, Y.C. Lin, K.H. Chen, L.C. Chen, S.T. Lin, Mechanical properties of nanocrystalline diamond films, *J. Appl. Phys.* 99 (12) (2006) 124302, <http://dx.doi.org/10.1063/1.2203428>.
- [30] G. Stoney, The tension of metallic films deposited by electrolysis, *Proc. R. Soc. Lond. Ser. A Math. Phys. Eng. Sci.* 82 (1909) 172–175, <http://dx.doi.org/10.1098/rspa.1909.0021>.
- [31] G.C.A.M. Janssen, M.M. Abdalla, F. van Keulen, B.R. Pujada, B. van Venrooy, Celebrating the 100th anniversary of the Stoney equation for film stress: Developments from polycrystalline steel strips to single crystal silicon wafers, *Thin Solid Films* 517 (6) (2009) 1858–1867, <http://dx.doi.org/10.1016/j.tsf.2008.07.014>.
- [32] P. Pobedinskas, J.-C. Bolsée, W. Dexters, B. Ruttens, V. Mortet, J. D’Haen, J.V. Manca, K. Haenen, Thickness dependent residual stress in sputtered AlN thin films, *Thin Solid Films* 522 (2012) 180–185, <http://dx.doi.org/10.1016/j.tsf.2012.08.015>.
- [33] M.A. Hopcroft, W.D. Nix, T.W. Kenny, What is the Young’s modulus of silicon? *J.*

- Microelectromech. Syst. 19 (2) (2010) 229–238, <http://dx.doi.org/10.1109/JMEMS.2009.2039697>.
- [34] H. Kato, M. Ogura, T. Makino, D. Takeuchi, S. Yamasaki, N-type control of single-crystal diamond films by ultra-lightly phosphorus doping, *Appl. Phys. Lett.* 109 (14) (2016) 142102, <http://dx.doi.org/10.1063/1.4964382>.
- [35] P.W. May, W.J. Ludlow, M. Hannaway, J.A. Smith, K.N. Rosser, P.J. Heard, Boron doping of microcrystalline and nanocrystalline diamond films: Where is the boron going? *MRS Online Proc. Lib.* 1039 (2007) 1703, <http://dx.doi.org/10.1557/proc-1039-p17-03>.
- [36] M. Sternberg, P. Zapoll, T. Frauenheim, D.M. Gruen, L.A. Curtiss, Molecular dynamics simulation of impurities in nanocrystalline diamond grain boundaries, *MRS Online Proc. Lib.* 593 (1999) 483–487, <http://dx.doi.org/10.1557/proc593-481>.
- [37] Y.-G. Lu, S. Turner, J. Verbeeck, S.D. Janssens, P. Wagner, K. Haenen, G. Van Tendeloo, Direct visualization of boron dopant distribution and coordination in individual chemical vapor deposition nanocrystalline B-doped diamond grains, *Appl. Phys. Lett.* 101 (4) (2012) 041907, <http://dx.doi.org/10.1063/1.4738885>.
- [38] N. Woehrl, T. Hirte, O. Posth, V. Buck, Investigation of the coefficient of thermal expansion in nanocrystalline diamond films, *Diam. Relat. Mater.* 18 (2) (2009) 224–228, <http://dx.doi.org/10.1016/j.diamond.2008.10.016>.
- [39] J. Philip, P. Hess, T. Feygelson, J.E. Butler, S. Chattopadhyay, K.H. Chen, L.C. Chen, Elastic, mechanical, and thermal properties of nanocrystalline diamond films, *J. Appl. Phys.* 93 (4) (2003) 2164–2171, <http://dx.doi.org/10.1063/1.1537465>.
- [40] C.-S. Wang, H.-C. Chen, H.-F. Cheng, I.-N. Lin, Origin of platelike granular structure for the ultrananocrystalline diamond films synthesized in H₂-containing Ar/CH₄ plasma, *J. Appl. Phys.* 107 (3) (2010) 034304, <http://dx.doi.org/10.1063/1.3296187>.
- [41] K.J. Sankaran, J. Kurian, H.C. Chen, C.L. Dong, C.Y. Lee, N.H. Tai, I.N. Lin, Origin of a needle-like granular structure for ultrananocrystalline diamond films grown in a N₂/CH₄ plasma, *J. Phys. D: Appl. Phys.* 45 (36) (2012) 365303, <http://dx.doi.org/10.1088/0022-3727/45/36/365303>.
- [42] J.A. Cuenca, K.J. Sankaran, P. Pobedinskas, K. Panda, I.-N. Lin, A. Porch, K. Haenen, O.A. Williams, Microwave cavity perturbation of nitrogen doped nanocrystalline diamond films, *Carbon* 145 (2019) 740–750, <http://dx.doi.org/10.1016/j.carbon.2018.12.025>.
- [43] Y. Cong, R.W. Collins, G.F. Epps, H. Windischmann, Spectroellipsometry characterization of optical quality vapor-deposited diamond thin films, *Appl. Phys. Lett.* 58 (8) (1991) 819–

- 821, <http://dx.doi.org/10.1063/1.104499>.
- [44] W. Fortunato, A.J. Chiquito, J.C. Galzerani, J.R. Moro, Crystalline quality and phase purity of CVD diamond films studied by Raman spectroscopy, *J. Mater. Sci.* 42 (2007) 7331–7336, <http://dx.doi.org/10.1007/s10853-007-1575-0>.
- [45] T. Izak, O. Babchenko, M. Varga, S. Potocky, A. Kromka, Low temperature diamond growth by linear antenna plasma CVD over large area, *Phys. Status Solidi b* 249 (12) (2012) 2600–2603, <http://dx.doi.org/10.1002/pssb.201200103>.
- [46] K.J. Sankaran, C.-J. Yeh, P.-Y. Hsieh, P. Pobedinskas, S. Kunuku, K.-C. Leou, N.-H. Tai, I.-N. Lin, K. Haenen, Origin of conductive nanocrystalline diamond nanoneedles for optoelectronic applications, *ACS Appl. Mater. Interfaces* 11 (28) (2019) 25388–25398, <http://dx.doi.org/10.1021/acsami.9b05469>.
- [47] X. Li, J. Perkins, R. Collazo, R.J. Nemanich, Z. Sitar, Investigation of the effect of the total pressure and methane concentration on the growth rate and quality of diamond thin films grown by MPCVD, *Diam. Relat. Mater.* 15 (11) (2006) 1784–1788, <http://dx.doi.org/10.1016/j.diamond.2006.09.008>.
- [48] G. Cicala, V. Magaletti, G. Senesi, G. Carbone, D. Altamura, C. Giannini, R. Bartali, Superior hardness and Young's modulus of low temperature nanocrystalline diamond coatings, *Mater. Chem. Phys.* 144 (3) (2014) 505–511, <http://dx.doi.org/10.1016/j.matchemphys.2014.01.027>.
- [49] Z. Sha, P. Branicio, V. Sorkin, Q. Pei, Y. Zhang, Effects of grain size and temperature on mechanical and failure properties of ultrananocrystalline diamond, *Diam. Relat. Mater.* 20 (10) (2011) 1303–1309, <http://dx.doi.org/10.1016/j.diamond.2011.08.012>.
- [50] P. Fallon, L. Brown, Analysis of chemical-vapour-deposited diamond grain boundaries using transmission electron microscopy and parallel electron energy loss spectroscopy in a scanning transmission electron microscope, *Diam. Relat. Mater.* 2 (5–7) (1993) 1004–1011, [http://dx.doi.org/10.1016/0925-9635\(93\)90265-4](http://dx.doi.org/10.1016/0925-9635(93)90265-4).
- [51] X. Xiao, J. Birrell, J.E. Gerbi, O. Auciello, J.A. Carlisle, Low temperature growth of ultrananocrystalline diamond, *J. Appl. Phys.* 96 (4) (2004) 2232–2239, <http://dx.doi.org/10.1063/1.1769609>.
- [52] H. Windischmann, G.F. Epps, Y. Cong, R.W. Collins, Intrinsic stress in diamond films prepared by microwave plasma CVD, *J. Appl. Phys.* 69 (4) (1991) 2231–2237, <http://dx.doi.org/10.1063/1.348701>.
- [53] T. Anthony, Stresses generated by impurities in diamond, *Diam. Relat. Mater.* 4 (12) (1995) 1346, [http://dx.doi.org/10.1016/0925-9635\(95\)00317-7](http://dx.doi.org/10.1016/0925-9635(95)00317-7).

[54] V. Buck, N. Woehrl, Tailoring the matrix in ultra-nanocrystalline diamond films, *Japan. J. Appl. Phys.* 47 (10) (2008) 8208–8213, <http://dx.doi.org/10.1143/jjap.47.8208>.